



Investigation of trapezoidal sharp-crested side weir discharge coefficients under subcritical flow regimes using CFD

Amir Ghaderi¹ · Mehdi Dasineh² · Saeed Abbasi¹ · John Abraham³

Received: 30 July 2019 / Accepted: 3 December 2019 / Published online: 12 December 2019
© The Author(s) 2019

Abstract

Side weirs are utilized to regulate water surface and to control discharge and water elevation in rivers and channels. Here, the discharge coefficient for trapezoidal sharp-crested side weirs (TSCSW) and their affecting parameters are numerically investigated. To simulate the hydraulic and geometric characteristics of TSCSWs, three weir crest lengths of 15 cm, 20 cm and 30 cm with lengths of 20 cm, 30 cm and 40 cm and with two different sidewall slopes are utilized. The results show that for constant P/B (P : weir height, B : main channel width), the depth of flow along the channel and weir decreases as the crest length increases. Also, with increasing P/y_1 ratio (P : weir height, y_1 : upstream flow depth), the discharge coefficient decreases for small crest lengths and increases for large crest lengths. The results show that for constant T/L ratio (T : passing flow width, L : side weir crest length), increasing the length, height and sidewall slope of a side weir will increase the discharge coefficient. It is observed that as the upstream Froude number increases for side weirs with longer crest lengths, the intensity of deviating flow and kinetic energy over the TSCSW will increase. Finally, some relations with high correlation factors are proposed for obtaining discharge coefficients using the dimensionless parameters of P/y_1 , T/L and Fr_1 . Based on proposed relations and sensitivity analysis, it is shown that T/L and P/y_1 are the most effective parameters for reducing the discharge coefficient reduction.

Keywords Side weir · Trapezoidal · Discharge coefficient · Upstream Froude number · FLOW-3D

Introduction

To control and maintain the flow in a channel or river, some discharge control structures such as side weirs are utilized. A side weir is built on the side of a main channel, and free spatially varying flow with decreasing discharge is the dominant regime over this hydraulic structure. Water is deviated from the main flow and sent to the side weir. Decreasing the ultimate (downstream) discharge in the main channel is the result of this action. It means if a flow with discharge (Q_1) crosses a side weir, its discharge will be reduced (Q_2) because of overspilling (Q_w) (see Fig. 1). Inadequate

assessment of a discharge coefficient and inappropriate hydraulic design of the structure may result in downstream damage or reduction in flow transmission capacity in the main channel.

The hydraulic behavior of side weirs has received considerable interest by many researchers. Hager (1987), Swamee et al. (1994), Borghei et al. (1999), Muslu (2002) and Torabi and Shafieifar (2015) investigated the hydraulic and geometric characteristics of side weir hydraulic structures. Coşar and Agaccioglu (2004) investigated the discharge coefficient for a triangular side weir on a curved channel. The results showed that for a curved channel, the path of maximum velocity and the secondary current created by the bend both cause a much greater deviation angle toward the side weir. Also triangular side weir discharge coefficients along the bend are greater than the values obtained in the straight channel. Venutelli (2008) proposed a method for reducing discharge coefficients for side weirs by repeating steps to solve the nonlinear flow equations. Hyung and Sop (2010) studied discharge coefficients of sharp-edge and broad-crested weirs using a De Marchi discharge coefficient.

✉ Amir Ghaderi
amir_ghaderi@znu.ac.ir

¹ Department of Civil Engineering, Faculty of Engineering, University of Zanjan, Zanjan, Iran

² Department of Civil Engineering, University of Maragheh, Maragheh, East Azerbaijan, Iran

³ School of Engineering, University of St. Thomas, St Paul, MN, USA

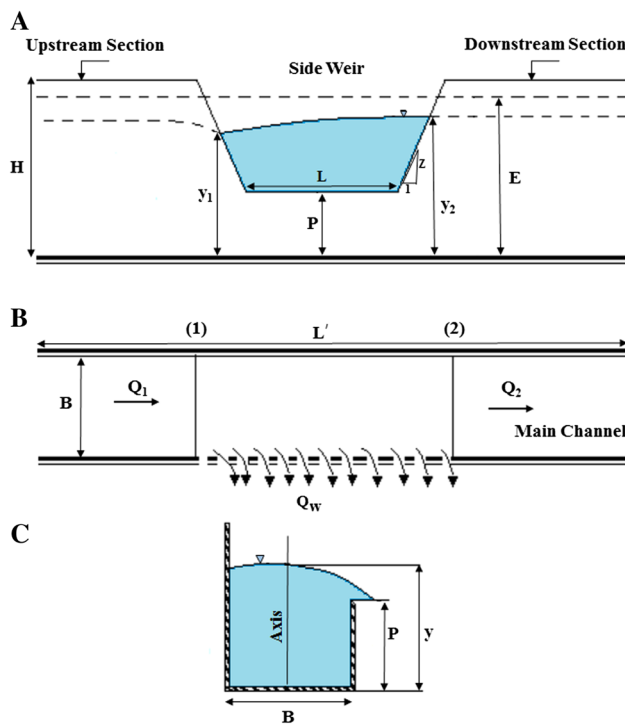


Fig. 1 General scheme of a TSCSW: (a) longitudinal section, (b) plan view and (c) cross-sectional view

The results showed the impact of upstream Froude number and weir height on wide open channels.

Rahimpour et al. (2011) investigated flow passing over a trapezoidal sharp-edged crest using both numerical and experimental techniques. The results showed that the discharge coefficient in subcritical flow is related to the Froude number, weir sidewall slope, ratio of crest length over the upstream depth and weir height over upstream depth of the side weir. Aydin and Emiroglu (2013) studied the discharge coefficient of flow over a side labyrinth spillway and its relevant parameters utilizing a finite volume method. They investigated the effect of parameters such as upstream Froude number, the ratio of weir height to its width and sidewall slope of the labyrinth side weir.

More recently, Abdollahi et al. (2017) investigated flow passing over labyrinth side spillways with some flow guiding obstacles; they used OpenFOAM software for the calculations. The results showed that the maximum discharge will occur when obstacles are perpendicular to the flow and are placed downstream of the spillway.

Despite numerous studies on the trapezoidal side spillways and their geometric and hydraulic characteristics, there are few investigations on the parameters that affect their discharge coefficients. In this paper, the discharge coefficient and relevant parameters in trapezoidal side weirs with various crest lengths, heights and wall slopes are investigated numerically using FLOW-3D.

Mathematical background

Dimensional analysis

The discharge coefficient of a TSCSW is related to geometric and hydraulic characteristics of the side weir and the fluid, respectively. Thus, we can write:

$$C_d = f_1(y_1, y_2, V_1, V_2, P, L, B, g, T, Z, H, L'), \quad (1)$$

which can be rewritten using Buckingham's Π theory:

$$C_d = f_2\left(\text{Fr}_1, \text{Re}, \text{We}, \frac{y_2}{y_1}, \frac{V_2}{V_1}, \frac{P}{y_1}, \frac{B}{y_1}, \frac{T}{L}, \frac{H}{L'}, S_0, Z\right). \quad (2)$$

Here, Fr_1 is the upstream Froude number, Re is the Reynolds number, We is the Weber number, P is the weir height, L is the side weir crest length, B is the main channel width, y_1 and y_2 are flow depths upstream and downstream, respectively, V_1 and V_2 are velocities upstream and downstream, respectively, Z is the sidewall slope, H is the main channel height, L' is the main channel length, S_0 is the channel bed slope, and T is the flow-passing width which equals $T = L + 2zy$. These dimensions and the physical situation are shown in a series of illustrations provided in Fig. 1.

The Reynolds and Weber numbers indicate the effects of viscosity and surface tension, respectively. The minimum depth of flow over the weir exceeds 3 cm, and the effect of surface tension can be neglected. In addition, the boundary layer is considered to be negligible and the viscosity effects are neglected. Also, the main channel width, length, height and longitudinal slope are constant and the ratios of y_2/y_1 and V_2/V_1 are small. Consequently, the impact of parameters of B , L' , H , S_0 , y_2/y_1 and V_2/V_1 is negligible. Finally, the following dimensionless parameters are expected to significantly affect the flow discharge coefficient:

$$C_d = f_3\left(\text{Fr}_1, \frac{P}{y_1}, \frac{T}{L}, Z\right). \quad (3)$$

Continuity equations, momentum and free surface

The dynamic behavior can be described by a set of equations known as the St. Venant equations (Daneshfaraz and Kaya 2008; Norouzi et al. 2019). FLOW-3D is used to solve complicated fluid dynamics problems; it is able to model a wide range of fluid flows. This software can be used to model 3D unsteady free surface flows with complicated geometry in which the volume of fraction (VOF) method is utilized. The governing equations are the Navier–Stokes (Daneshfaraz et al. 2019; Ghaderi and Abbasi 2019) and continuity equations. The general form of the continuity equation is:

$$V_F \frac{\partial \rho}{\partial t} + \frac{\partial}{\partial x}(\rho u A_x) + R \frac{\partial}{\partial y}(\rho v A_y) + \frac{\partial}{\partial z}(\rho w A_z) + \xi \frac{\rho u A_x}{x} = R_{DIF} + R_{SOR} \tag{4}$$

Here, V_F is the free volume coefficient; ρ is density and R is the source term. The general forms of the 3D momentum equations are:

$$\frac{\partial u}{\partial t} + \frac{1}{V_F} \left[u A_x \frac{\partial u}{\partial x} + v A_y \frac{\partial u}{\partial y} + w A_z \frac{\partial u}{\partial z} \right] - \xi \frac{A_y v^2}{x V_F} = -\frac{1}{\rho} \frac{\partial P}{\partial x} + G_x + f_x - \frac{R_{SOR}}{\rho V_F} (u - u_w - \delta u_s) \tag{5}$$

$$\frac{\partial v}{\partial t} + \frac{1}{V_F} \left[u A_x \frac{\partial v}{\partial x} + v A_y \frac{\partial v}{\partial y} + w A_z \frac{\partial v}{\partial z} \right] + \xi \frac{A_y u v}{x V_F} = -\frac{1}{\rho} \left(R \frac{\partial P}{\partial y} \right) + G_y + f_y - \frac{R_{SOR}}{\rho V_F} (v - v_w - \delta v_s) \tag{6}$$

$$\frac{\partial w}{\partial t} + \frac{1}{V_F} \left[u A_x \frac{\partial w}{\partial x} + v A_y \frac{\partial w}{\partial y} + w A_z \frac{\partial w}{\partial z} \right] = -\frac{1}{\rho} \frac{\partial P}{\partial z} + G_z + f_z - \frac{R_{SOR}}{\rho V_F} (w - w_w - \delta w_s) \tag{7}$$

In the above equations, P is pressure; G_x , G_y and G_z are volumetric accelerations; and f_x , f_y and f_z are the mass accelerations. In FLOW-3D, unlike some numerical software such as HEC-RAS, the free surface profile is estimated using $F(x, y, z)$ (Ghaderi et al. 2019). This function shows the fluid volume in the cell and is expressed as:

$$\frac{\partial F}{\partial t} + \frac{1}{V_F} \left[\frac{\partial}{\partial x}(F A_x u) + \frac{\partial}{\partial y}(F A_y v) + \frac{\partial}{\partial z}(F A_z w) \right] = 0. \tag{8}$$

In the above equation, A is the average ratio of flow area along x -, y - and z -directions, u , v , w are average velocities along x , y , z and F is the fluid ratio function which takes on values between 0 and 1. If $F=0$, the cell is completely full of air, and if $F=1$, the cell is full of water. The free surface occurs where $F=0.5$ (Daneshfaraz et al. 2016a).

Turbulence model

The RNG $k-\epsilon$ (Renormalized Group) turbulence model is used to simulate the flow domain because of its acceptable accuracy and success in prior studies (Aydin and Emiroglu 2013; Azimi and Shabanlou 2018; Daneshfaraz and Ghaderi 2017; Daneshfaraz et al. 2016b). The RNG $k-\epsilon$ model is a two-equation model that is expressed as:

$$\frac{\partial}{\partial t}(\rho k) + \frac{\partial(\rho k u_i)}{\partial x_i} = \frac{\partial}{\partial x_j} \left(\alpha_k \mu_{eff} \frac{\partial k}{\partial x_j} \right) + G_k + G_b - \rho \epsilon - Y_M + S_k \tag{9}$$

$$\frac{\partial}{\partial t}(\rho \epsilon) + \frac{\partial(\rho \epsilon u_i)}{\partial x_i} = \frac{\partial}{\partial x_j} \left(\alpha_s \mu_{eff} \frac{\partial \epsilon}{\partial x_j} \right) + C_{1s} - \frac{\epsilon}{k} (G_k + G_{3s} G_b) + C_{2\epsilon} \rho \frac{\epsilon^2}{k} - R_\epsilon + S_\epsilon \tag{10}$$

In these equations, k is the turbulent kinetic energy; ϵ is the turbulence dissipation rate, G_k is production of turbulent kinetic energy due to velocity gradient, G_b is turbulent

kinetic energy production from buoyancy and Y_M is turbulence dilation oscillation distribution (Yakhot et al. 1992; Lai and Wu 2019). In the above equations, $\alpha_k = \alpha_s = 1.39$, $C_{1s} = 1.42$ and $C_{2\epsilon} = 1.6$ are model constants. The terms S_k and S_ϵ are sources terms for k and ϵ , respectively. Turbulence viscosity μ_t is defined using the following equations. In fact, the turbulent viscosity is added to the molecular viscosity to obtain, μ_{eff} , effective viscosity. It accounts for both molecular and turbulent effects. The following equations provide detail on how the effective viscosity is determined.

$$d \left(\frac{\rho^2 k}{\sqrt{\epsilon} \mu} \right) = 1.72 \frac{\nu}{\sqrt{\nu^3 - 1 + C_\nu}} \tag{11}$$

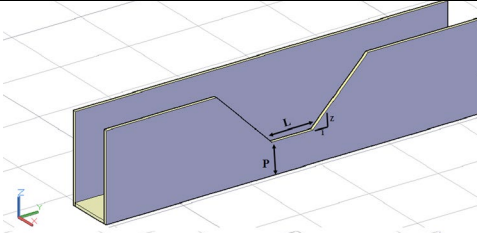
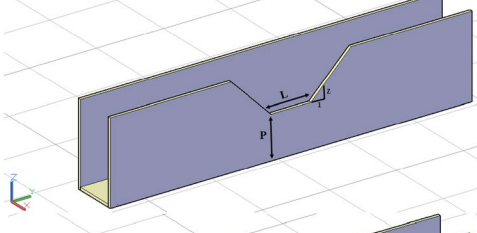
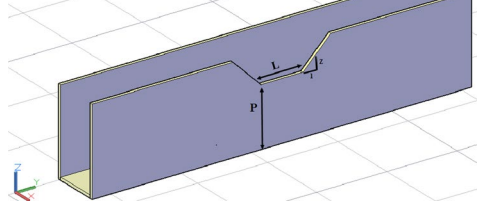
$$\nu = \mu_{eff} / \mu, C_\nu = 100. \tag{12}$$

Methods and materials

Geometric model

In the present study, three crest lengths of 15, 20 and 30 cm with heights of 20, 30 and 40 cm and sidewall slopes of $z=1$ and $z=2$ are utilized to simulate the hydraulic and geometric characteristics affecting the discharge coefficient. The results of case $L/B=0.667$, $P=40$ cm and $z=1$ are validated

Table 1 Geometric parameters of the present study

Trapezoidal sharp-edged side weir (TSCSW)	Sidewall slope, Z	Weir crest length, L (cm)	Weir height, P (cm)	Main channel depth, y (cm)	Froude no. Fr	Input discharge, Q (L/s)
	1, 2	15, 20, 30	20	26–60	> 0.9	> 70
	1, 2	15, 20, 30	30	26–60	> 0.9	> 70
	1, 2	15, 20, 30	40	26–60	> 0.9	> 70

with the experimental results of (Tabrizi et al. 2015). The experiments were conducted in a rectangular flume with the length, width, and depth of 20, 0.6, and 0.6 m, respectively. The flume is made of 0.02-m-thick plexiglass with a bed slope of 0.001. With used plexiglass, the influence of sidewall effects is considered to be negligible based upon studying with Moradinejad et al. (2019). Table 1 shows the hydraulic and geometric conditions of the present study.

Solution domain characteristics and boundary conditions

Several computational meshes were utilized to select the appropriate mesh. As listed in Table 2, a comparison between the calculated and measured free surface profiles was performed. Based on this mesh refinement study, a computational mesh with 1,987,703 elements was selected for

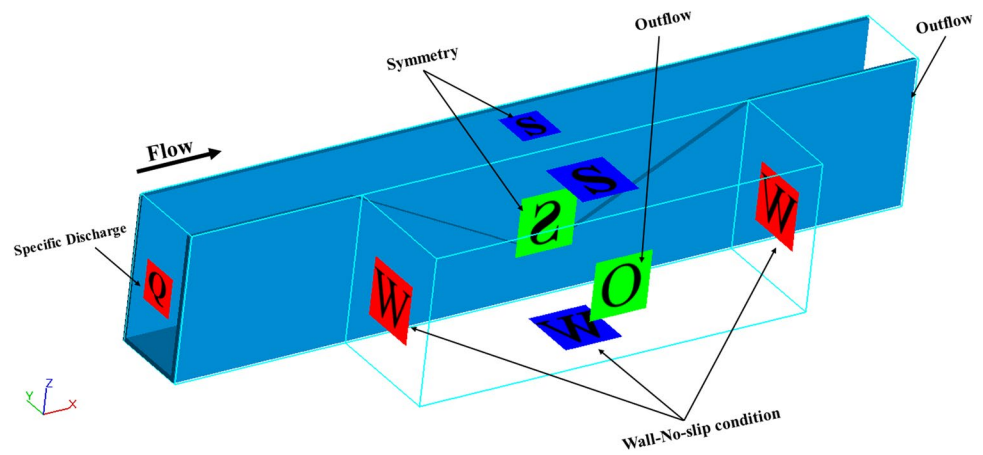
Table 2 Mesh sensitivity analysis for the present study

Test no.	Total mesh number	Max aspect ratio	MAPE (%)* $100 \times \frac{1}{n} \sum_1^n \left \frac{X_{exp} - X_{num}}{X_{exp}} \right $	RMSE (cm)** $\sqrt{\frac{1}{n} \sum_1^n (X_{exp} - X_{num})^2}$
1	784,929	1	27.33	1.48
2	1,059,566	1	21.21	1.06
3	1,499,343	1	15.56	0.79
4	1,987,703	1	8.73	0.38
			5	A system with high processing capability is needed

*Denotes mean absolute percentage error; X_{exp} , experimental value of X ; X_{num} , numerical value of X ; and n , count of data

**Denotes root-mean-square error; X_{exp} , experimental value of X ; X_{num} , numerical value of X ; and n , count of data

Fig. 2 Boundary condition labels for the TSCSW model



further calculations; the selected appropriate mesh results in a relative error, RMSE and maximum aspect ratio of 8.73%, 0.38 and 1, respectively. The same mesh was utilized to all models of this research.

A symmetry (S) boundary condition was used for the upper boundary; specific discharge (Q) was used for the input flow and outlet (O) conditions for flow for the downstream boundary. Wall (W) boundary conditions were assigned for the bed and the sidewalls to enforce a no-slip condition. Figure 2 shows annotations of the applied boundary conditions of the TSCSW on the FLOW-3D model domain.

Results and discussion

Verification of numerical model and laboratory results

To validate the model, a comparison is made between the calculated and experimental results. In order to quantify the error, Eq. 13 was used. The simulation was completed in a sufficient duration to ensure steady conditions were achieved, and then, the comparison was made. This method is similar to that of (Zahabi et al. 2018):

$$E = \left| \frac{(Cd_E - Cd_N)}{Cd_E} \right| \times 100. \tag{13}$$

The term E is the relative error percentage, Cd_E is the experimental discharge coefficient and Cd_N is the numerical counterpart. Figure 3 and Table 3 show discharge coefficients and errors. Good agreement is found between the numerical and experimental data, and the experimental and numerical data represent a nearly similar trend.

It can be seen that the largest difference between the data relates to $P/y_1 = 0.743$ (side weir height over the depth of upstream flow) and is equal to 7.13%.

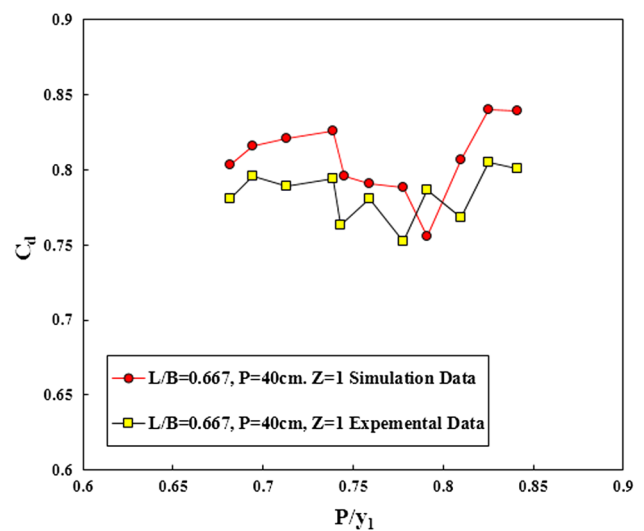


Fig. 3 Comparison of numerical and experimental discharge coefficients ($P = 40$ cm, $L/B = 0.667$, $Z = 1$)

Table 3 Comparison of numerical and experimental discharge coefficients ($P = 40$ cm, $L/B = 0.667$, $Z = 1$)

P/y_1	Experimental data (Tabrizi et al. 2015)	Numerical data FLOW-3D	Relative errors (%)	RMSE
0.682	0.781	0.803	2.82	0.037
0.694	0.796	0.816	2.51	0.038
0.713	0.789	0.821	3.89	0.031
0.713	0.794	0.829	4.22	0.035
0.743	0.743	0.796	7.13	0.039
0.759	0.781	0.809	3.58	0.037
0.778	0.751	0.788	4.93	0.038
0.791	0.787	0.824	4.70	0.039
0.810	0.768	0.807	5.08	0.039
0.825	0.805	0.840	4.35	0.040
0.841	0.801	0.846	5.62	0.045

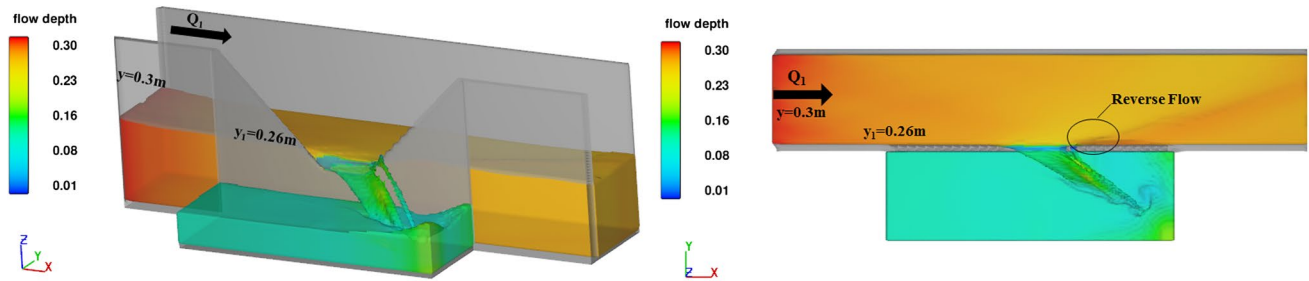
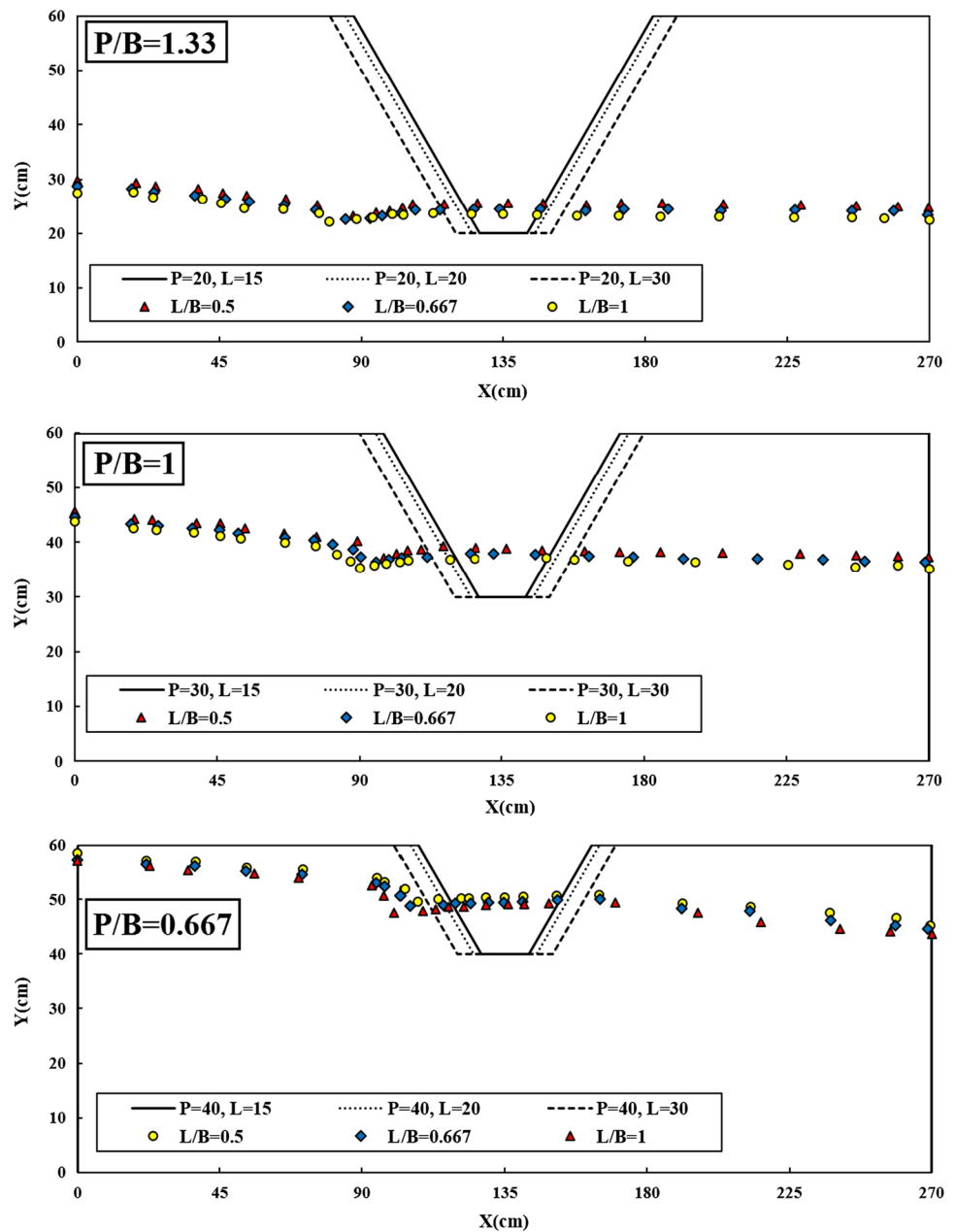


Fig. 4 Flow passing over a TSCSW with $P=20$ cm

Fig. 5 Free surface profile of flow passing over a TSCSW ($P/B=1.33, 1$ and 0.667)



Free surface profile flow over a TSCSW

Figure 4 shows the flow passing over a TSCSW with a height of 20 cm. It is seen that the flow is spatially varied and the depth of flow reduces as a part of flow abandons the main channel. Also, the flow passing adjacent to the sidewall collides with the wall at an angle before returning to the main stream. As a result, an increase in the depth of the main channel can be observed.

Figure 5 shows the free surface profile of flow passing over a TSCSW for three different ratios of P/B . It can be seen that for various values of P/B , the water surface profile experiences a reduction and later re-enhancement in depth, which is caused by the flow passing to the side channel. By increasing the weir's height, a secondary current will be created that reduces the water surface fluctuation and the flow surface profile experiences less curvature.

Side weir length (L) effects

Figure 6 shows discharge coefficients for a TSCSW with P/y_1 for different heights of $P=20, 30$ and 40 cm. It is seen that there is very little trend in the results, in general, for any particular dataset. A slight decline is observed for $P/B=1$ and $L/B=0.5$ case, while a slight increase is found for $P/B=1.33$ and $L/B=1$.

On the other hand, there is a notable spread that separates the individual datasets. It is evident as the weir's length increases, for constant values of P/y_1 , the value of C_d increases. With increasing P/y_1 , the discharge coefficient of the TSCSW for $L=15$ cm decreases. This length provides the shortest crest. This reduction in discharge coefficient is in accordance with findings of (Agaccioglu and Yuksel 1998; Emiroglu et al. 2010) who carried out research on rectangular sharp-edged side weirs with $L/B=0.5$. However, for side weirs with a crest length of $L=20$ cm, the discharge coefficient is almost constant, while it increases for $L=30$ cm. The intensity of secondary flow and deviating

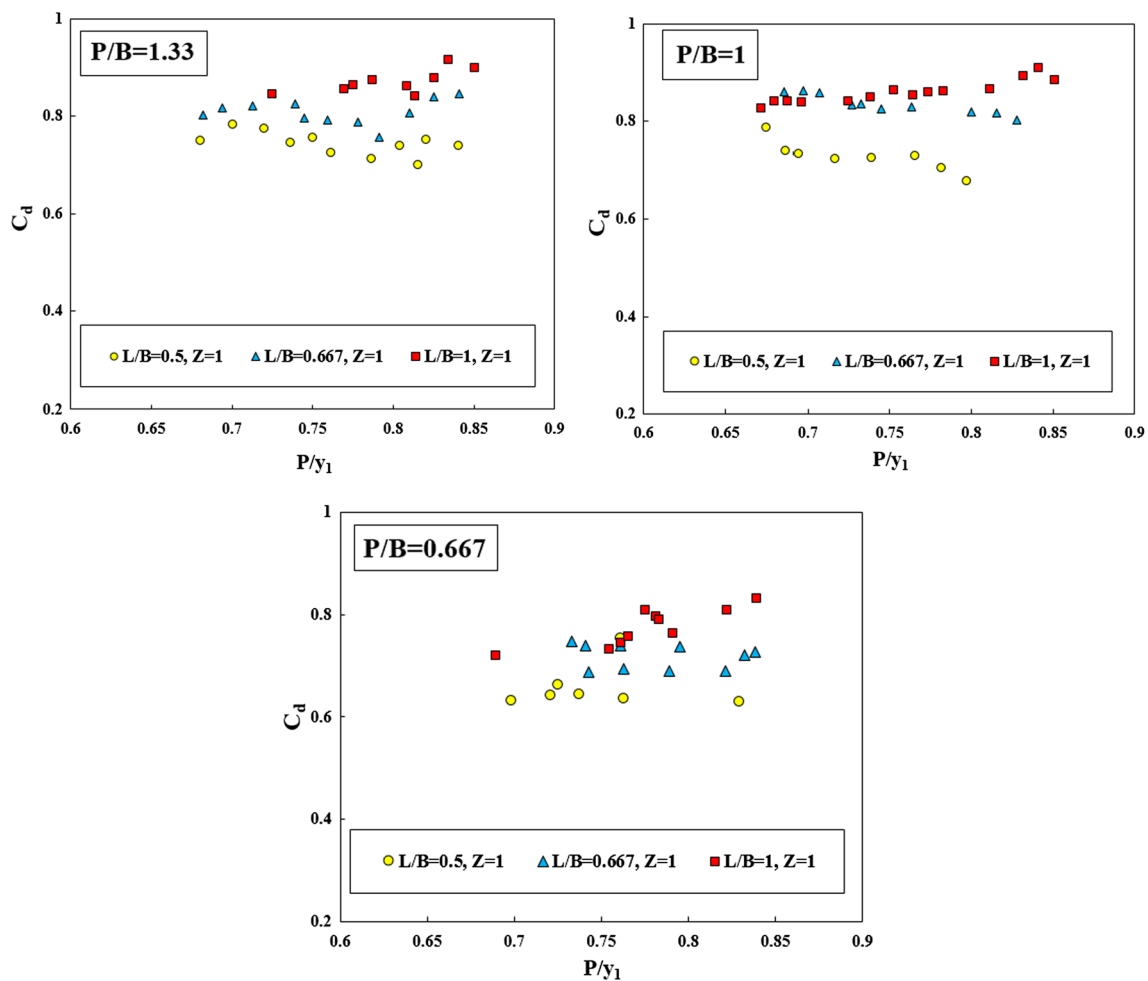


Fig. 6 Variation in discharge coefficient with P/y_1 (weir height to upstream depth) ($P/B=1.33, 1$ and 0.667)

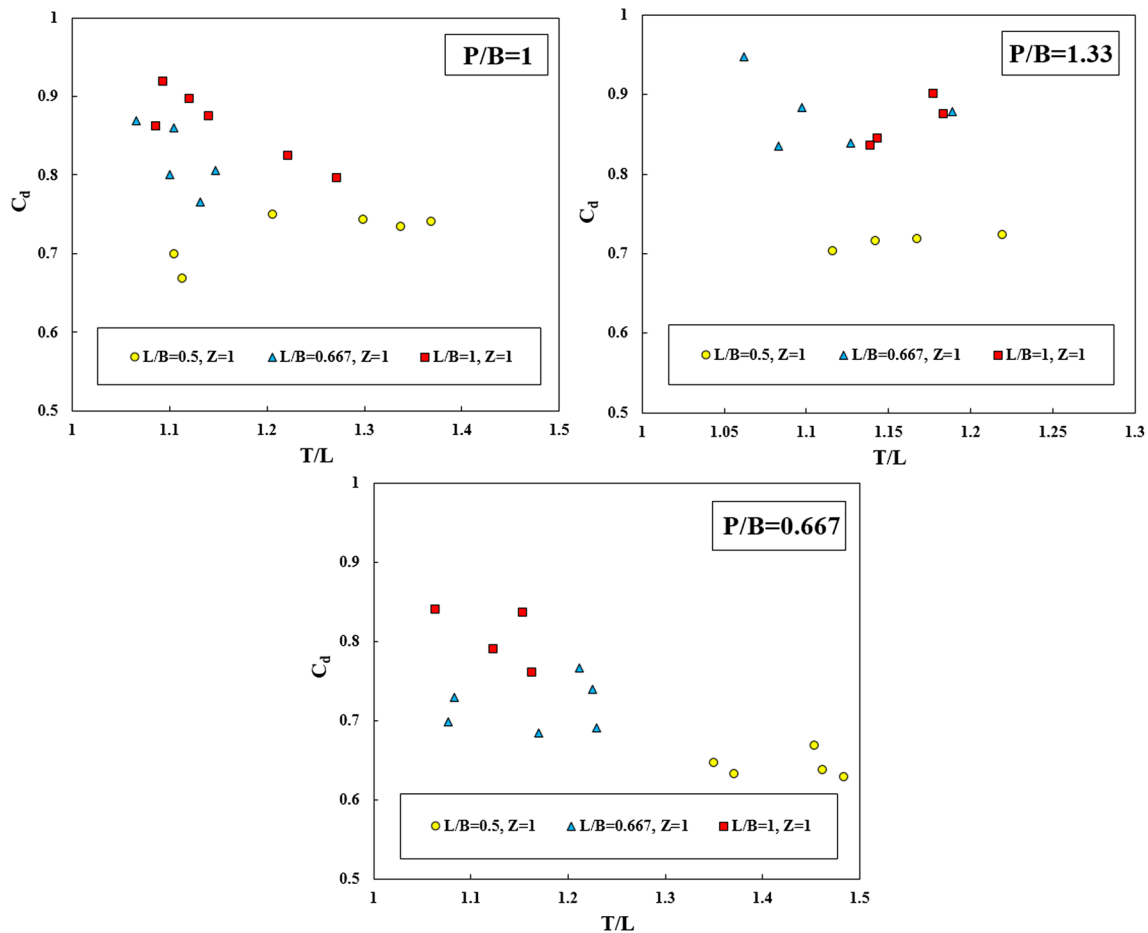


Fig. 7 Variation in C_d with T/L (passing flow width to weir crest length) in $z=1$ ($P/B=1.33, 1$ and 0.667)

flow from the main channel increases the discharge coefficient and crest length.

Effects of passing flow width (T)

Figure 7 shows the variation in discharge coefficient C_d in TSCSW and T/L (passing flow width over weir crest length) for weir heights of $P=20, 30$ and 40 cm and $21 < T < 32$ cm.

It is seen that increasing the weir height at constant T/L will increase the discharge coefficient. With increasing T/L for L/B values of 0.5 and 1 , the discharge coefficient exhibits a decreasing trend in all three models and results in a weir crest length reduction.

Effects of upstream Froude number (Fr_1)

Figure 8 shows variations in discharge coefficient C_d with upstream Froude number (Fr_1) for different values of P/y_1 .

It is seen that the discharge coefficient increases with increasing P/y_1 ratio and the weir crest length. This is due to increased weir height and to the reduction in the secondary

current from the main channel to the side weir. The lower the height of the weir, the larger the return flow and the earlier the submergence of side weir occurs. Also, for constant values of P/y_1 , increasing the crest length will reduce the influence of the deviated flow and will increase the discharge of the side weir passing flow.

Sidewall slope of TSCSW (Z)

Figure 9 shows the variation in discharge coefficient with P/y_1 and T/L ratios for two different sidewall slopes. It can be observed that different ratios of T/L and P/y_1 and increasing the sidewall slope increase the discharge coefficient. Increasing the ratios of T/L and P/y_1 at two sidewall slopes of TSCSW causes a decrease in the discharge coefficient. However, there are variations among discharge coefficients at two sidewall slopes. Some equations are proposed in Table 4 that can be used to estimate the discharge coefficient for different values in the slopes.

The 80–20 rule is utilized in proposing the above equations. With this approach, the coefficients and powers are

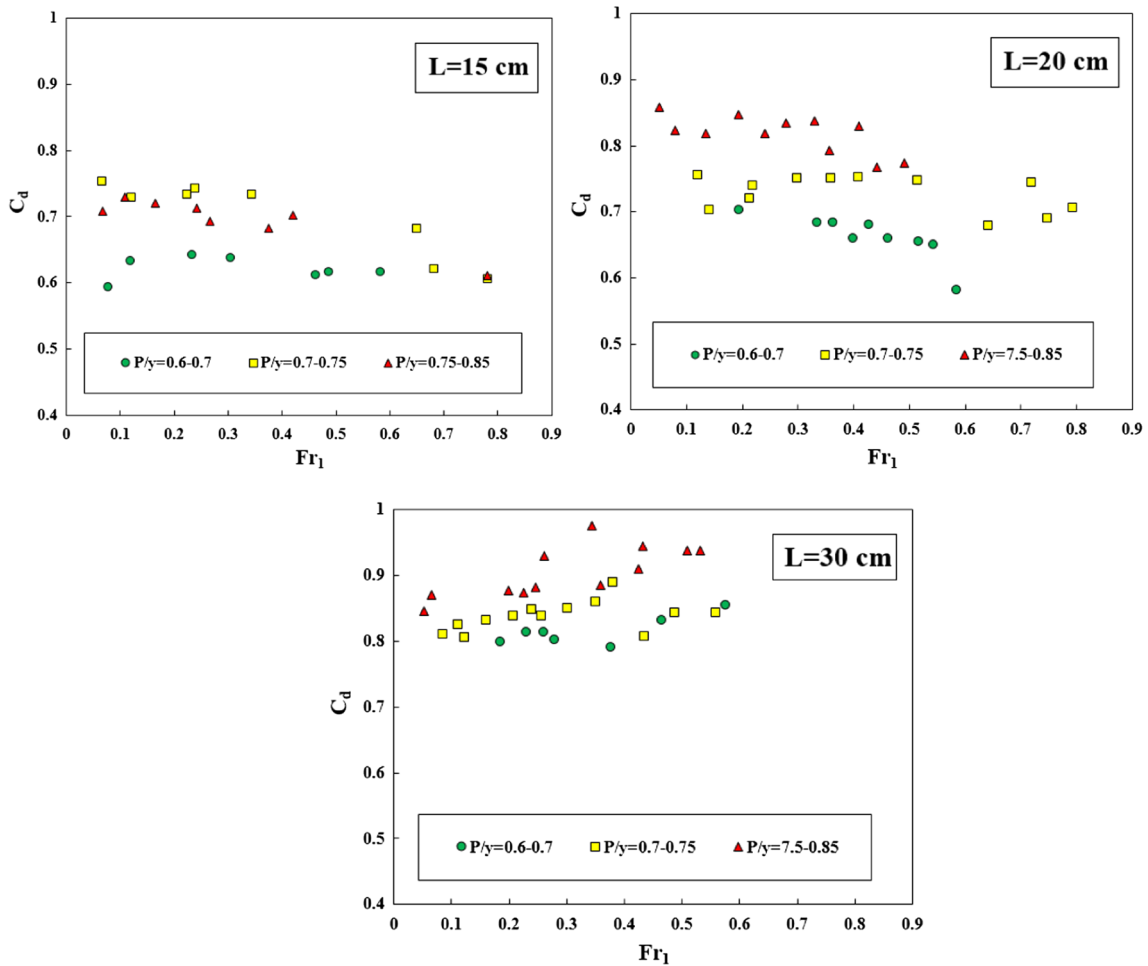


Fig. 8 Variations in C_d (discharge coefficient) with upstream Froude number (Fr_1) ($L = 15, 20$ and 30 cm)

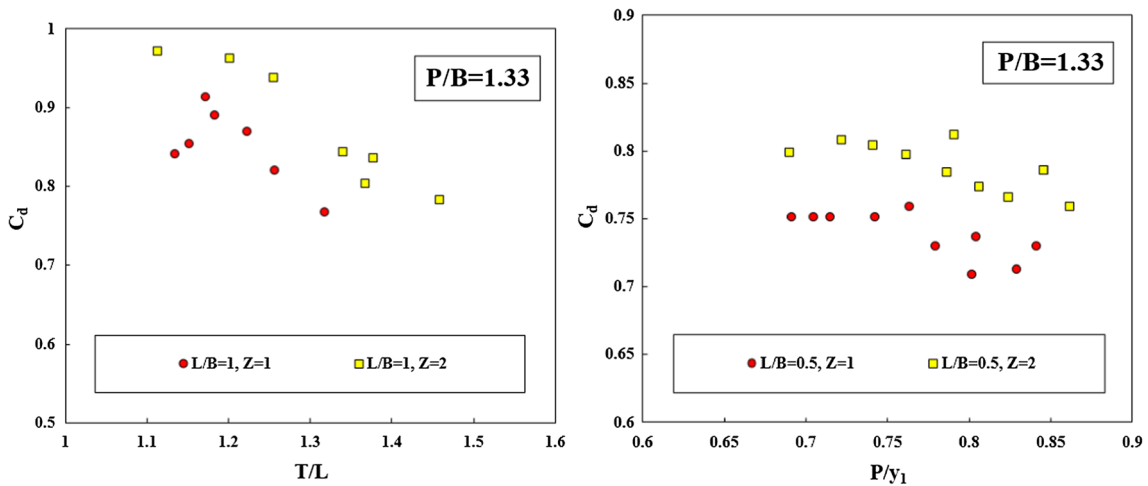


Fig. 9 Variations in discharge coefficient with P/y_1 and T/L for two different sidewall slopes ($P/B = 1.33, Z = 1, 2$)

Table 4 Proposed equations for discharge coefficients for various sidewall slopes

	Proposed equation	Sidewall slope (Z)	Determination coefficients (R^2)	Relative error (%)	RMSE
1	$C_d = 0.048(Fr_1)^{0.566} + 2.489\left(\frac{P}{y_1}\right)^{0.351} - 2.540\left(\frac{T}{L}\right)^{0.738}$	1	0.986	4.520	0.077
2	$C_d = 0.337(Fr_1)^{0.347} + 2.564\left(\frac{P}{y_1}\right)^{0.415} - 3.179\left(\frac{T}{L}\right)^{0.875}$	2	0.991	5.221	0.079
3	$C_d = 0.359(Fr_1)^{1.385} + 1.699\left(\frac{P}{y_1}\right)^{0.774} - 2.539\left(\frac{T}{L}\right)^{1.252} + 0.673\left(\frac{Z}{Z+1}\right)^{1.018}$	1, 2	0.997	3.921	0.063

Table 5 Sensitivity analysis for the general equation of discharge coefficient

	Percent reduction				Percent increment				Dimensionless parameters
	20%	40%	60%	80%	30%	50%	70%	90%	
C_d									
	0.256	0.179	0.103	0.040	0.513	0.623	0.738	0.858	Fr_1
	1.429	1.144	0.836	0.489	2.081	2.325	2.562	2.792	P/y_1
	-1.920	-1.339	-0.806	-0.338	-3.526	-4.218	-4.935	-5.671	T/L
	0.536	0.400	0.264	0.131	0.879	1.017	1.155	1.293	$Z/Z+1$

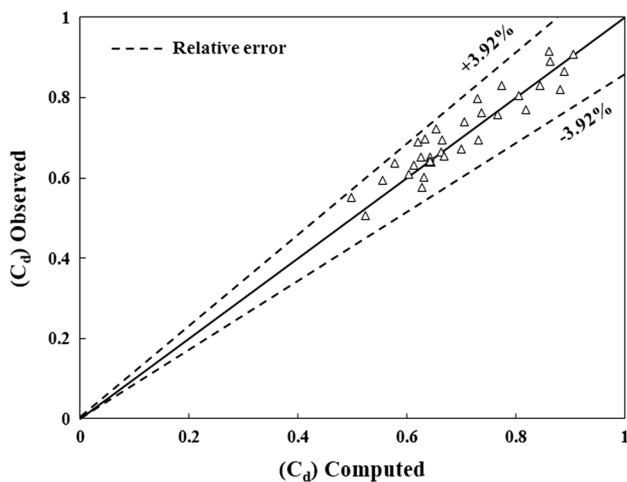


Fig. 10 Variations in numerical data with estimates from (main equation, Eq. 3) for the TSESW model

derived using 80% of the data and the other 20% are used to validate the coefficients and powers. The relative error and the RMSE are calculated for that 20% of the data. Table 5 and Fig. 10 show the sensitivity analysis and numerical data variations with estimated data from the primary proposed equation (Eq. 3). According to Table 5, it can be seen that the T/L parameter has the greatest effect on discharge coefficient. Also, P/y_1 has the largest effect on increases in the discharge coefficient. According to Fig. 10, it is seen that there is a good agreement among the numerical and estimated data.

From the results that have been presented, some clear conclusions can be drawn.

1. The profile of flow passing through the TSCSW at different ratios of P/B first experiences a reduction at the beginning and then slightly increases further downstream. The reason for the reduction is due to flow separation caused by fluid entering the TSCSW. With increasing height of the weir, the water level alteration decreases and the flow surface profile experiences less curvature.
2. For constant ratios of P/y_1 , the discharge coefficient increases with increasing the crest length. Also, with increasing values of P/y_1 , the discharge coefficient for the TSCSW with a crest length of $L = 15$ cm is descending. On the other hand, the discharge coefficient is almost constant for $L = 20$ cm and increases for $L = 30$ cm. The reason for the increase is the intensity of secondary flow and the flow diverting from the main channel.
3. For constant ratios of T/L , the discharge coefficient is decreases for $L/B = 0.5$ and 1 in all three models, which means the crest length could be reduced.
4. With increasing Froude number upstream of a large crested TSCSW, the deviation of flow and the kinetic energy of the flow through the side weir increase. For side weirs with smaller crest lengths, the discharge coefficient at high Froude numbers decreases because of rapid submergence of the weir.
5. Sidewall slope increments will increase the discharge coefficient. This is due to the increase in the deviation angle and the kinetic energy.

6. Some dimensionless equations were proposed to estimate the variations in discharge coefficient of TSCSW with P/y_1 , T/L and Fr_1 .
7. Sensitivity analysis of the main discharge coefficient equation was performed, and this analysis showed that changes to T/L and P/y_1 have the greatest impact on discharge coefficient.

Conclusion

In the present study, the discharge coefficient of trapezoidal sharp-edged side weirs (TSCSW) and their affecting parameters are investigated using FLOW-3D. In this research, three trapezoidal sharp-edged weirs with crest lengths of 15, 20 and 30 cm, heights of 20, 30 and 40 cm and sidewall slopes of $Z=1$ and 2 are utilized. The numerical model was first compared with experimental results to demonstrate the suitability of the calculations for adequately capturing the flow features.

Subsequently, changes to numerous independent parameters were made using the computational software to determine their effect on the flow. Changes included modifications to the P/B ratio, P/y_1 , crest length, T/L , Froude number and slopes. New correlating equations are provided that allow the prediction of discharge coefficients for various values of the influencing parameters.

Compliance with ethical standards

Conflict of interest The authors declare that they have no conflict of interest.

Open Access This article is licensed under a Creative Commons Attribution 4.0 International License, which permits use, sharing, adaptation, distribution and reproduction in any medium or format, as long as you give appropriate credit to the original author(s) and the source, provide a link to the Creative Commons licence, and indicate if changes were made. The images or other third party material in this article are included in the article's Creative Commons licence, unless indicated otherwise in a credit line to the material. If material is not included in the article's Creative Commons licence and your intended use is not permitted by statutory regulation or exceeds the permitted use, you will need to obtain permission directly from the copyright holder. To view a copy of this licence, visit <http://creativecommons.org/licenses/by/4.0/>.

References

- Abdollahi A, Kabiri-Samani A, Asghari K, Atoof H, Bagheri S (2017) Numerical modeling of flow field around the labyrinth side-weirs in the presence of guide vanes. *ISH J Hydraul Eng* 23(1):71–79
- Agaccioglu H, Yuksel Y (1998) Side weir flow in curved channels. *J Irrig Drain Eng ASCE* 124(3):163–175
- Aydin MC, Emiroglu ME (2013) Determination of capacity of labyrinth side weir by CFD. *Flow Meas Instrum* 29:1–8
- Azimi H, Shabanlou S (2018) U-shaped channels along the side weir for subcritical and supercritical flow regimes. *ISH J Hydraul Eng* 138:1–11
- Borghei M, Jalili MR, Ghodsian M (1999) Discharge coefficient for sharp-crested side weir in subcritical flow. *J Hydraul Eng ASCE* 125(10):1051–1056
- Coşar A, Agaccioglu H (2004) Discharge coefficient of a triangular side-weir located on a curved channel. *J Irrig Drain Eng* 130(5):410–423
- Daneshfaraz R, Ghaderi A (2017) Numerical investigation of inverse curvature ogee spillway. *Civ Eng J* 3(11):1146–1156
- Daneshfaraz R, Kaya B (2008) Solution of the propagation of the waves in open channels by the transfer matrix method. *Ocean Eng* 35(11–12):1075–1079
- Daneshfaraz R, Ghahramanzadeh A, Ghaderi A, Joudi AR, Abraham J (2016a) Investigation of the effect of edge shape on characteristics of flow under vertical gates. *J Am Water Works Assoc* 108(8):425–432
- Daneshfaraz R, Joudi AR, Ghahramanzadeh A, Ghaderi A (2016b) Investigation of flow pressure distribution over a stepped spillway. *Adv Appl Fluid Mech* 19(4):811
- Daneshfaraz R, Minaei O, Abraham J, Dadashi S, Ghaderi A (2019) 3-D numerical simulation of water flow over a broad-crested weir with openings. *ISH J Hydraul Eng* 25:1–9
- Emiroglu ME, Kaya N, Agaccioglu H (2010) Discharge capacity of labyrinth side weir located on a straight channel. *J Irrig Drain Eng ASCE* 136(1):37–46
- Ghaderi A, Abbasi S (2019) CFD simulation of local scouring around airfoil-shaped bridge piers with and without collar. *Sādhanā* 44(10):216
- Ghaderi A, Daneshfaraz R, Dasineh M (2019) Evaluation and prediction of the scour depth of bridge foundations with HEC-RAS numerical model and empirical equations (Case Study: Bridge of Simineh Rood Miandoab, Iran). *Eng J* 23(6):279–295
- Hager WH (1987) Lateral outflow over side weirs. *J Hydraul Eng ASCE* 113(4):491–504
- Hyung PM, Sop RD (2010) Development of discharge formula for broad crested side weir. *J Korea Water Resour Assoc* 43(6):525–531
- Lai YG, Wu KA (2019) Three-dimensional flow and sediment transport model for free-surface open channel flows on unstructured flexible meshes. *Fluids* 4(1):18
- Moradinejad A., Saneie M., Ghaderi A, Shahri SMZ (2019) Experimental study of flow pattern and sediment behavior near the intake structures using the spur dike and skimming wall. *Appl Water Sci* 9(8):195
- Muslu Y (2002) Lateral weir flow model using a curve fitting analysis. *J Hydraul Eng ASCE* 128(7):712–715
- Norouzi, R, Daneshfaraz, R, Ghaderi A (2019) Investigation of discharge coefficient of trapezoidal labyrinth weirs using artificial neural networks and support vector machines. *Appl Water Sci* 9(7):148
- Rahimpour M, Keshavarz Z, Ahmadi M (2011) Flow over trapezoidal side weir. *Flow Meas Instrum* 22(6):507–510
- Swamee PK, Pathak SK, Ali MS (1994) Side weir analysis using elementary discharge coefficient proceeding. *J Irrig Drain Div ASCE* 120(4):743–755
- Tabrizi H, Fatahi R, Ghorbani B (2015) Laboratory investigation on discharge coefficient of trapezoidal sharp crested side weirs. *Iran Water Res J* 9(1):123–133 [In Persian, available in English upon request]
- Torabi MA, Shafieefar M (2015) An experimental investigation on the stability of foundation of composite vertical breakwaters. *J Mar Sci Appl* 14(2):175–182

- Venutelli ME (2008) Method of solution of non-uniform flow with the presence of rectangular side weirs. *J irrig Drain Eng ASCE* 134(6):840–846
- Yakhot V, Orsarg SA, Thangam S, Gatski TB, Speziale CG (1992) Development of turbulence models for shear flows by a double expansion technique. *Phys Fluids* 4(7):1510–1520

- Zahabi H, Torabi M, Alamatian E, Bahiraei M, Goodarzi M (2018) Effects of geometry and hydraulic characteristics of shallow reservoirs on sediment entrapment. *Water* 10(12):1725

Publisher's Note Springer Nature remains neutral with regard to jurisdictional claims in published maps and institutional affiliations.